Fine Control Over the Size of Surfactant–Polyelectrolyte Nanoparticles by Hydrodynamic Flow Focusing

ARTICLE *in* ANALYTICAL CHEMISTRY · MAY 2013

Impact Factor: 5.64 · DOI: 10.1021/ac4006155 · Source: PubMed

5 AUTHORS, INCLUDING:

Guillaume Tresset
Université Paris-Sud 11
28 PUBLICATIONS **691** CITATIONS
SEE PROFILE

Anniina Salonen
Université Paris-Sud 11
53 PUBLICATIONS **516** CITATIONS
SEE PROFILE

Ming Ni
Institute of Bioengineering and Nanotechnology
31 PUBLICATIONS **437** CITATIONS
SEE PROFILE

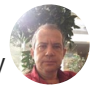

Ciprian Iliescu
Agency for Science, Technology and Research …
130 PUBLICATIONS **1,525** CITATIONS
SEE PROFILE

analytical chemistry

Article

pubs.acs.org/ac

Fine Control Over the Size of Surfactant–Polyelectrolyte Nanoparticles by Hydrodynamic Flow Focusing

Guillaume Tresset,*[,†] Catalin Marculescu,[‡] Anniina Salonen,[†] Ming Ni,[§] and Ciprian Iliescu*[,§]

[†]Laboratoire de Physique des Solides, Université Paris-Sud, CNRS, 91405 Orsay, France

[‡]National Institute for Research and Development in Microtechnologies, IMT-Bucharest, 077190 Bucharest, Romania

[§]Institute of Bioengineering and Nanotechnology, 31 Biopolis Way, The Nanos 04-01, 138669 Singapore, Singapore

ABSTRACT: Synthesis of surfactant–polyelectrolyte nanoparticles was carried out in a microfluidic device with a fine control over the size and the polydispersity. An anionic polysaccharide (sodium carboxymethylcellulose, CMC) solution was focused using a cationic surfactant (dodecyl trimethylammonium bromide, DTAB) solution in a microfluidic channel at selected ratios of flow rates and reagent concentrations. The methodology ensured a controlled mixing kinetics and a uniform distribution of charges at the mixing interface. The resulting nanoparticles exhibited remarkably well-defined and repeatable size distributions, with hydrodynamic diameters tunable from 50 up to 300 nm and polydispersity index around 0.1 in most cases. Microfluidic-assisted self-assembly may be an efficient way to produce well-controlled polyelectrolyte-based nanoparticles suitable for colloidal science as well as for gene delivery applications.

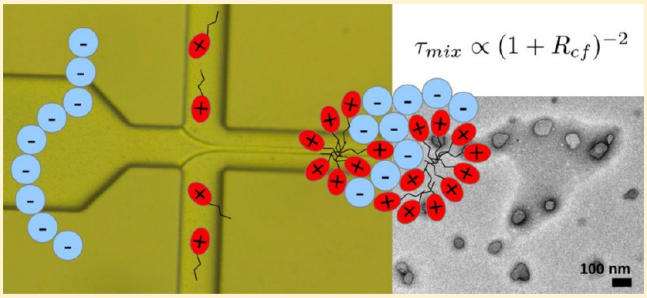

Nanoparticles made up of oppositely charged polyelectrolytes and surfactants in aqueous solutions have attracted a growing interest in colloidal science.[1,2] They are frequently used in many industrial applications, including food, cosmetics, detergents, and paints to name just a few. Moreover, these nanoparticles are surface-active and can stabilize foams and thin liquid films.[3] They also hold great promise in medicine as biosensors and nanovectors for drug delivery applications.[4,5] The addition of surfactants to a solution of polyelectrolytes leads to a discrete coil–globule conformational transition[6] of the polyelectrolyte chains (Figure 1). The transition arises from a combination of electrostatic attraction between the positively charged surfactant headgroups (in red in Figure 1) and the negatively charged monomers of the polyelectrolytes (in cyan in Figure 1) and hydrophobic interactions between the alkyl chains of the surfactant molecules (broken lines in Figure 1) favoring their accumulation. Depending on the concentration and contour length of the polyelectrolyte as well as on the mixing time, several polyelectrolyte chains may be entangled and compacted at a time giving rise to large nanoparticles. In general, the size of the resulting nanoparticles is poorly controlled because the assembly process is driven by kinetics and the system may quickly become trapped into a metastable state.[7] Yet, nanoparticles with well-defined morphologies are required in most applications, especially for delivery purposes in which the nanoparticles need to diffuse within the tissues or through the blood vessel walls.[5]

Recent developments in microfluidics have enabled the chemical synthesis of soft matter micro- and nanoparticles with excellent control of size, composition, morphology, as well as size distribution.[8,9] Qi et al. reported the fabrication of multilayer polyelectrolyte nanocarriers based on surface acoustic wave atomization.[10] Synthesis of ultrasmall (<5 nm) metallic nanocrystals in microfluidic channels using gas-evolving reducing agents was described by Khan and Duraiswamy.[11] Fabrication of lipid nanoparticles by microfluidic mixing in serpentine channels[12] or using the microvortex generated at the confluence of microfluidic channels[13] was also reported recently. One particular method resorts to microfluidic hydrodynamic flow focusing to precisely control the convective–diffusive mixing of miscible liquids at nanometer length scales which determine the formation of nanoparticles.[14] Notable achievements include formation of lipid vesicles,[15] liposome–hydrogel hybrid nanoparticles,[16] cross-linked alginate nanoparticles,[17] monodisperse chitosan-based nanoparticles,[18] and nanoprecipitation of diblock copolymers.[19]

Here we report the use of microfluidic hydrodynamic flow focusing to achieve a fine control over the size of surfactant–polyelectrolyte nanoparticles. Unlike bulk methods of assembly, microfluidics permitted us to obtain a broad variety of nanoparticle sizes in a highly reproducible manner by adjusting the flow rates and the concentrations of reagents brought in contact. Most specific features of the microfluidic approach include a tunable mixing time down to a few tens of milliseconds and a uniform distribution of charges at the mixing interface ensuring homogeneous electrostatic attractions

Received: February 27, 2013
Accepted: May 10, 2013
Published: May 28, 2013

   dx.doi.org/10.1021/ac4006155 | *Anal. Chem.* 2013, 85, 5850–5856

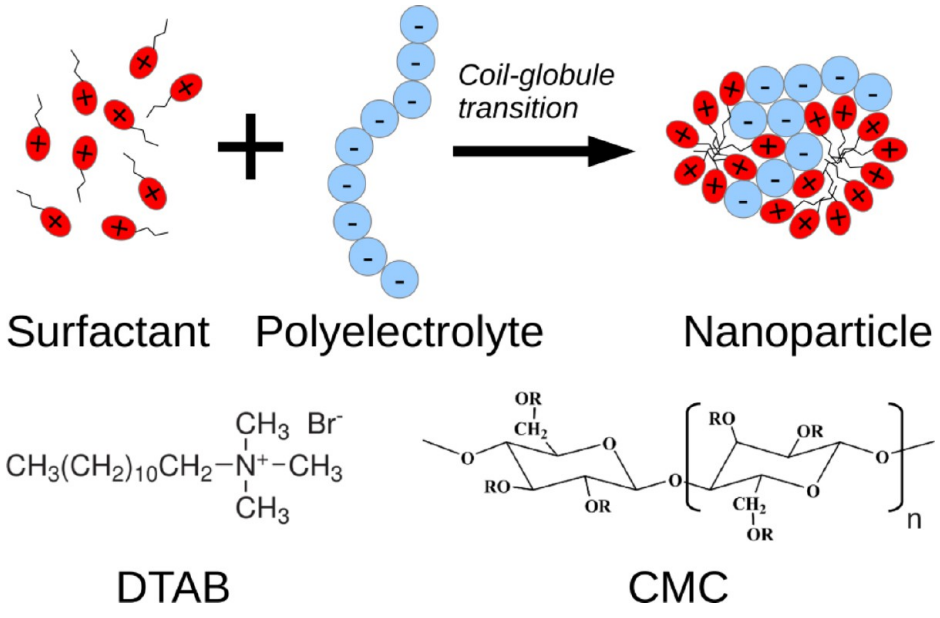

Figure 1. Coil–globule transition of a polyelectrolyte in the presence of oppositely charged surfactant. Surfactant molecules are represented with their cationic headgroups in red and their alkyl chains as broken lines. The polyelectrolyte is shown as a string of beads (cyan) representing its monomers, each of which carries negative charges. Note that the resulting nanoparticle may contain several polyelectrolyte chains. The chemical structures of DTAB (surfactant) and CMC (polyelectrolyte) used in this study are given at bottom. R = −H or R = $-CH_2COONa$ depending on the degree of substitution.

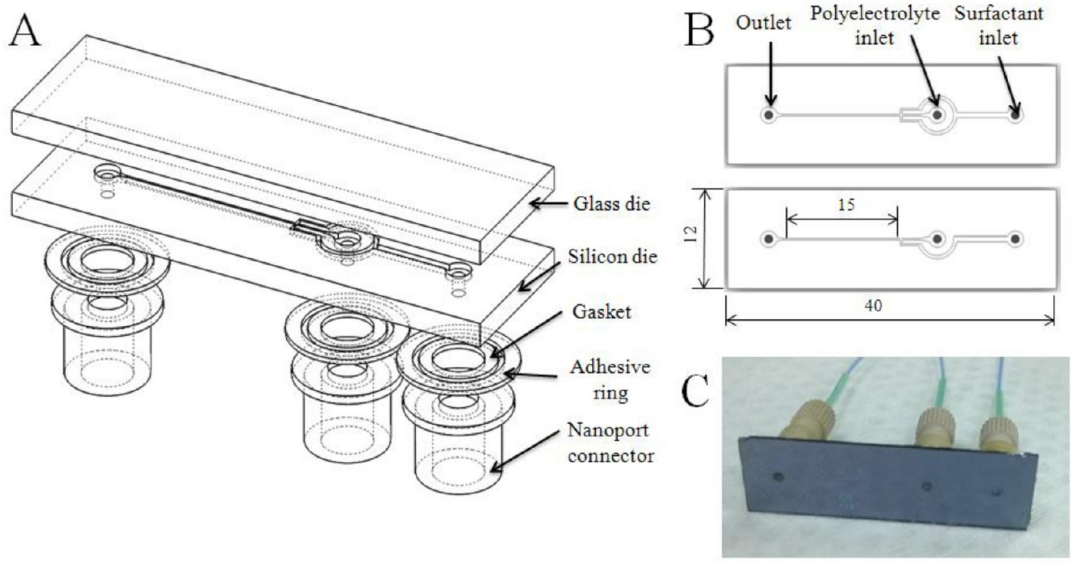

Figure 2. Microfluidic device for hydrodynamic flow focusing. (A) Exploded view depicting the various parts of the device made in a combination of glass and silicon: a silicon die on which the channel was patterned as well as the inlet/outlet holes; a glass die bonded to the silicon that assured the ceiling of the channel; three connectors (polyelectrolyte inlet, surfactant inlet, and outlet) bonded with an O-ring adhesive tape, the sealing between the fluidic connectors and the silicon die being assured by a gasket. (B) Layouts of the microfluidic channels for both versions of the device: with central focusing of the polyelectrolyte stream in the center of the channel, and with side focusing. (C) Photograph showing the bottom of the device and its fluidic connections.

between oppositely charged reagents. Two different microfluidic configurations were tested, and both yielded nanoparticles with well-defined and narrow size distributions. The morphology of nanoparticles was further investigated by transmission electron microscopy, and the observed sizes were in agreement with light scattering measurements. To our knowledge, this study is the first to report the synthesis of surfactant–polyelectrolyte nanoparticles by using hydrodynamic flow focusing in a microfluidic device.

EXPERIMENTAL SECTION

Reagents. Sodium carboxymethylcellulose (CMC, Figure 1) was supplied by Aqualon Hercules with a minimum purity of 99.5%. The degree of substitution was DS = 1.23, and the molecular weight 171 kDa. Dodecyl trimethylammonium bromide (DTAB, Figure 1) was purchased from Sigma-Aldrich with a purity >99%.

Device Structure. Figure 2 gives a representation of the microfabricated device. Unlike a number of microfluidic

dx.doi.org/10.1021/ac4006155 | Anal. Chem. 2013, 85, 5850–5856

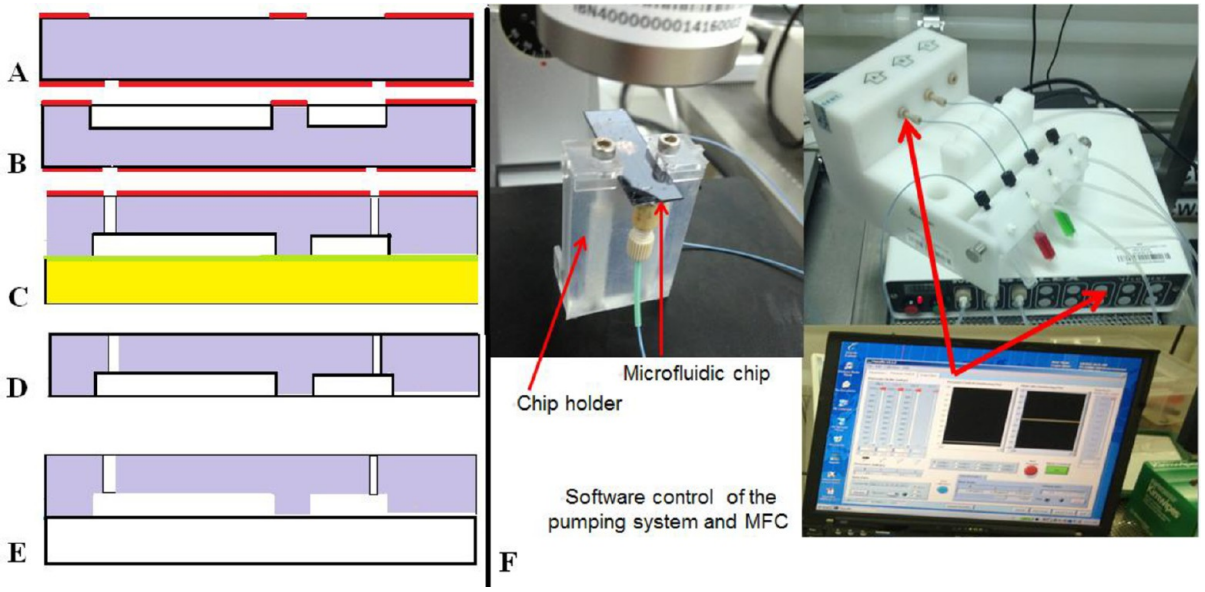

Figure 3. Main steps of the fabrication process and experimental setup: (A) processing of the SiO_2 masks (in red) on a silicon wafer (in purple) for the microfluidic channels and inlet/outlet holes; (B) DRIE etching of the channels; (C) DRIE etching of inlet/outlet holes; the silicon wafer is temporarily bonded with wax onto a dummy silicon wafer (in yellow); (D) thermal oxidation yielding a 150 nm thick SiO_2 layer on silicon surface; (E) anodic bonding of the silicon wafer to glass. (F) Photographs showing the experimental setup including the chip and its holder, the pumping system, and a screen shot of the control software.

channels fabricated in poly(dimethylsiloxane) (PDMS), we opted for glass/silicon[20,21] so as to confer a hydrophilic nature to the walls, and thus to minimize the nonspecific interactions with the hydrocarbonated chain of surfactants. The device consists of two dies (silicon and glass, Figure 2A) bonded together. The microfluidic structure was processed in silicon for a good control of the channel dimension as well as for a symmetrical cross section. The inlet and outlet holes were also processed on silicon die. Three Nanoport connectors (Upchurch Scientific) were mounted on the silicon surface. Notice that the surfactant channel was split for a uniform pressure drop and a symmetrical focusing (central focusing) of the polyelectrolyte stream (Figure 2B). A second version of the device presents an asymmetrical focusing (side focusing), the polyelectrolyte flowing along the wall of the channel. The dimensions of the chip were 40 mm × 12 mm, and the focusing channel had a cross section of 60 μm × 40 μm (width × depth) for a length of 15 mm. An optical image of the device is presented in Figure 2C. The device was easily cleaned by simply flushing with deionized water for a few minutes. The cleaning process was performed before each experiment.

Device Fabrication. A 4 in., 300 μm thick, double-side polished silicon wafer with (100) crystallographic orientation was used for the fabrication of the microfluidic channels. The wafer was cleaned in piranha (H_2SO_4/H_2O_2) for 20 min at 120 °C. PECVD (plasma-enhanced chemical vapor deposition) SiO_2 was deposited as a mask for patterning silicon into microfluidic channels (top side 500 nm thick) and for inlet/outlet holes (bottom side 2 μm thick). The transfer of the mask on the PECVD layer was performed using a positive photoresist AZ7220 (Clariant) and an RIE (reactive ion etching) process (SPTS equipment) using CHF_3/O_2. After its transfer onto the SiO_2 layer, the photoresist mask was removed in a photoresist striper. A first deep RIE process (for the microfluidic channel) was performed on an ICP DRIE system (Alcatel AMS100) using SF_6/O_2 as processing gases (Figure 3B). The etch depth (time-controlled) was 40 μm. After plasma cleaning in O_2 for removing the passivation layer, the structure of the channel was covered with a 200 nm thick PECVD TEOS (tetraethyl orthosilicate) layer. The main role of this layer was to protect the integrity of the microfluidic channel during the processing of the inlet/outlet holes by a classical deep RIE.[22] The silicon wafer was mounted on a dummy silicon wafer using a temporary bonding with wax. To avoid the melting of wax, the process was performed at −10 °C (the small modification of the etching profile did not affect the functionality of the device). Debonding of the wax was performed on a hot plate. The residual wax was removed in hot NMP (*N*-methylpyrrolidone) in an ultrasonic tank. Both SiO_2 masks and the TEOS layer were finally removed in a BOE solution (buffer oxide etch). A final 150 nm thick SiO_2 layer was thermally grown in a Tystar furnace (Figure 3D). This layer generated a hydrophilic surface in the microfluidic channel. After oxidation, the processed silicon wafer was anodically bonded onto a glass wafer (Corning 7740, Figure 3E). The wafer was diced, and Nanoport connectors were mounted for fluidic connections.

Nanoparticle Assembly. The setup is presented in Figure 3F. Two channels from a MFCS-FLEX pumping system (from Fluigen, France) were used for nanoparticle assembly in microfluidic channel. The system was equipped with mass flow controllers for each channel (up to 50 μL/min), and a software allowed fine-tuning of the applied pressure to the liquid for a uniform control of the flow rate. During the experiment, the flow rate in the microfluidic channels was maintained constant by tuning the applied pressure. The flow rate of the polyelectrolyte was maintained constant for most of experiments at 4 μL/min while the flow rate for surfactant was varied in order to obtain ratios of flow rates of 4, 6, 8, and 12. After each experiment the microfluidic channel was flushed with deionized water for 5 min for complete removal of the residual particles and contaminants.

dx.doi.org/10.1021/ac4006155 | *Anal. Chem.* 2013, 85, 5850−5856

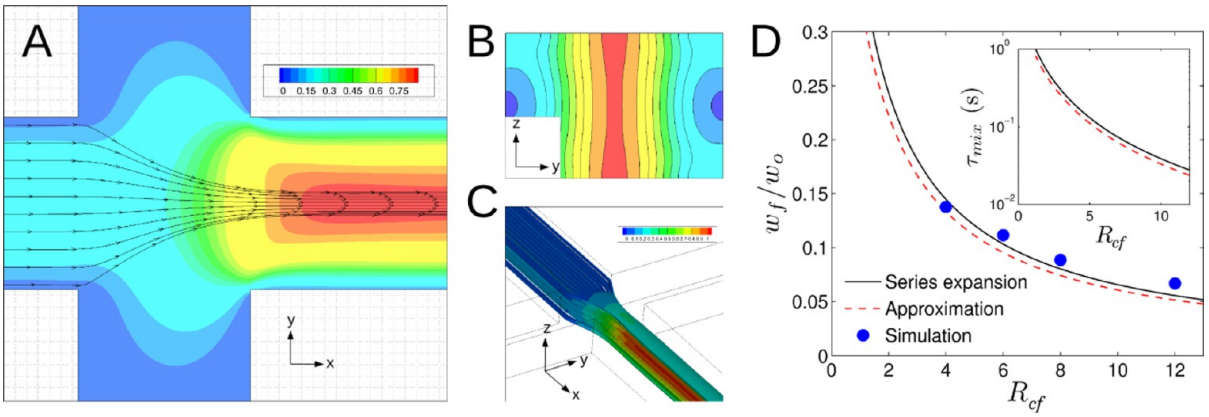

Figure 4. Calculated hydrodynamic flow focusing effect in a microchannel. The width of the channel was 60 μm, and its height was 40 μm. (A–C) Numerical 3D simulation with a ratio of flow rates R_{cf} = 12. (A) Top and (B) cross-sectional views of the streams taken at midheight and at the outlet of the simulated microchannel, respectively. The colors give the local fluid velocity normalized to its maximal value. The arrows indicate the flow direction. (C) Perspective view of the focused stream only, with the same color code as in panels B and C. (D) Width of the focused stream ω_f normalized to the width of the microchannel ω_0 vs the ratio of flow rates R_{cf}. ω_f was averaged over the height of the microchannel and measured at the exit. The plot compares values given by numerical simulations (blue discs) and eq 1 with a full series expansion for γ (black line) or with the approximation $\gamma \approx 3/2$ (dashed red line). The inset shows the mixing time τ_{mix} calculated from eqs 1 and 2.

Nanoparticle Characterizations. Nanoparticle sizes were measured by dynamic light scattering (DLS) with a Nano ZS-90 instrument (Malvern Instruments). Data were collected at a backscattering angle of 173° with temperature maintained at 25 °C. Size analysis was carried out by the cumulants method and the polydispersity index (PDI) was estimated accordingly. All the measurements were taken in triplicate and subsequently averaged. Note that the size of nanoparticles estimated by dynamic light scattering is actually a hydrodynamic diameter, namely, the diameter of hard spheres that diffuse at the same rate as the nanoparticles.[23] The hydrodynamic diameter includes a hydration layer and shape effects, and it varies as the dimensions of the nanoparticles.

Nanoparticles were imaged by transmission electron microscopy (TEM) with a JEOL 2011 microscope. An amount of 5 μL of sample was deposited on a carbon grid for 5 min and washed out. A drop of 1% (v/w) ammonium molybdate was then put on the grid during 30 s for negative staining of the sample. After thorough drying of the grid, it was introduced into the microscope and imaged at 200 kV with a magnification of ×10 000–20 000. Images were collected with a UltraScan 2 × 2k CCD camera from Gatan.

Computer Simulations. The numerical 3D geometry and the structured orthogonal mesh were generated using GAMBIT preprocessor (ANSYSR), consisting of 1 339 200 hexahedral finite volumes. The three-dimensional (3D) pressure-driven flow in the microchannel configuration was simulated using the FLUENT CFD package (ANSYSR). The code computed the isothermal laminar flows of the Newtonian working fluids, with double precision and with a 10^{-10} convergence criterion. The numerical simulations were performed using a constant flow rate for the central stream and variable flow rates for the focusing streams.

RESULTS AND DISCUSSION

Simulations and Analytical Considerations Regarding Hydrodynamic Flow Focusing. Parts A–C of Figure 4 illustrate the strong focusing effect on the central stream through a numerical simulation. It shows that the focused stream heading to the outlet was dramatically pinched by the lateral flows. As a result, it could be virtually mixed in a short time since the length scale over which the fluids had to diffusively mix was reduced.

Let Q_A and Q_B the flow rates of the central (polyelectrolyte) and lateral (surfactant) streams, respectively. By solving the Navier–Stokes equation in a rectangular geometry with the assumptions that the fluids are Newtonian and incompressible and the flows are laminar, the ratio of flow rates $R_{cf} = 2Q_B/Q_A$ for this central focusing configuration verifies the relationship

$$R_{cf} = \frac{1}{\gamma}\frac{\omega_0}{\omega_f} - 1 \qquad (1)$$

where ω_f and ω_0 are the widths of the focused and outlet streams, respectively, and γ is a complex function of ω_f, ω_0 as well as of h the height of the microchannel. γ can be expressed analytically through a series expansion.[24] In the high aspect ratio limit ($h \to \infty$) and for $\omega_f/\omega_0 \ll 1$, it verifies the approximation $\gamma \approx 3/2$. Equation 1 revealed that the width of the focused stream could be reduced by a factor 20 upon the application of a ratio of flow rates R_{cf} of 13 (Figure 4D). Note that the approximation $\gamma \approx 3/2$ yielded a solution of eq 1 very close to that obtained with a series expansion, and both expressions were in agreement with our numerical simulations with no adjustable parameter (Figure 4D). As a result, the time required for the focusing fluid to diffuse transversely across the tightly focused stream is considerably shortened. A rough estimate of the mixing time is given by

$$\tau_{mix} \approx \frac{\omega_f^2}{4D} \approx \frac{\omega_0^2}{9(1+R_{cf})^2 D} \qquad (2)$$

where D denotes the diffusion constant. The last approximation in eq 2 arises from the high aspect ratio limit of the microchannel. For small molecules like surfactants, the hydrodynamic radius of which is a few nanometers at most, D is around 10^{-10} m^2/s. The inset of Figure 4D depicts τ_{mix} as a function of R_{cf} and shows that the high aspect ratio approximation closely follows the variations obtained with a series expansion for γ. Thanks to the rapid decrease of τ_{mix} as R_{cf}^{-2} and provided the dimensions of our microchannel, τ_{mix} can be tuned from one second down to a few tens of milliseconds over a decade in R_{cf}.

dx.doi.org/10.1021/ac4006155 | Anal. Chem. 2013, 85, 5850–5856

Hydrodynamic Side Focusing versus Central Focusing. We began by a comparison between a configuration in central focusing as described previously with a configuration in side focusing. The side focusing involved only two streams: the polyelectrolyte stream was this time sandwiched between the surfactant stream coming laterally and the opposite wall of the microfluidic channel (Figure 5A). At first approximation, the

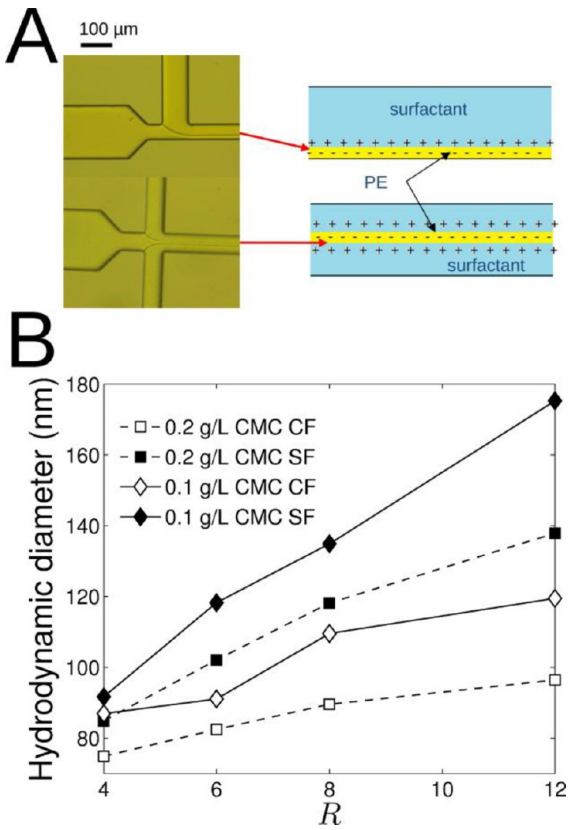

Figure 5. Comparison between central focusing (CF) and side focusing (SF). (A) Photographs of the microchannels showing side focusing (top) and central focusing (bottom) along with a schematic depicting the streams containing surfactant (blue) and polyelectrolyte (yellow). (B) Hydrodynamic diameter of nanoparticles obtained by both methods of focusing vs $R = R_{cf}$ or R_{sf}. CMC concentration was 0.1 g/L (diamond, solid line) and 0.2 g/L (square, dashed line). DTAB concentration was 5 mM. Full symbols are related to side focusing and empty symbols to central focusing.

width of the focused stream decreased moderately with the ratio of flow rates (here, $R_{sf} = Q_B/Q_A$), i.e., $\omega_f \approx \omega_0/(3R_{sf})^{1/2}$, so did the mixing time which thereby scaled as R_{sf}^{-1}. For example, in a 60 μm wide channel and with a ratio of flow rates $R_{sf} = 12$, the mixing time in side focusing was more than 10-fold higher than with central focusing. Therefore, the comparison between both configurations allowed us to shed light on the kinetic effects of mixing, the final concentrations of reagents being identical.

Nanoparticles were assembled in deionized water by focusing a stream containing an anionic polyelectrolyte, sodium carboxymethylcellulose (CMC; Figure 1), with a stream of a cationic surfactant, dodecyl trimethylammonium bromide (DTAB; Figure 1), at given ratios of flow rates $R = R_{cf}$ or R_{sf} depending on the configuration. Figure 5B shows the hydrodynamic diameter of nanoparticles produced in both configurations. Clearly, there was a systematic increase of the nanoparticle size in side focusing, which emphasized the importance of kinetic effects to assemble the nanoparticles. Such a difference was observed for two CMC concentrations and for a variety of ratios of flow rates. For instance, we measured a size increase by ~46% at $R = 12$ for 0.1 and 0.2 g/L of CMC when we switched from central to side focusing (DTAB concentration was 5 mM in both cases). Besides, the increase in size seemed more pronounced at larger R.

These results can be understood in terms of assembly at the interface. The nanoparticles formed near the interface separating positively and negatively charged reagents grew by consecutive adsorption of cations and polyanions so as to constantly balance the charge of the growing particles. This principle is exploited, for example, in surface chemistry to fabricate layered polymeric multicomposites by successive adsorption of oppositely charged polyelectrolytes.[25] The adsorption time scale τ_{ad} over which this process occurred could be as low as a few milliseconds due to the strength of electrostatic interactions. Once the interface disappeared because of the diffusion, the free reagents in minority were depleted and the growth process ended. Subsequently, for given final concentrations of reagents—therefore, fixed R since it varied the final concentrations as discussed below—a long mixing time ($\tau_{mix} \gg \tau_{ad}$) gave rise to large nanoparticles and vice versa. This trend was also reported for the self-assembly of amphiphilic block copolymers upon a rapid change of solvent quality.[26] In the following experiments, only central focusing was considered because small nanoparticles are preferred in practice.

Influence of the Surfactant-to-Polyelectrolyte Ratio of Flow Rates. Figure 6A shows the size of assembled

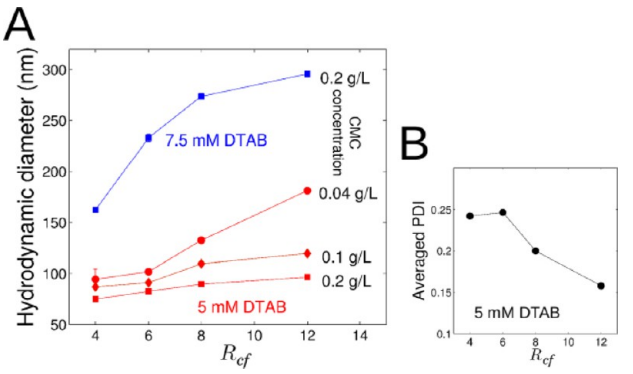

Figure 6. Size control of DTAB−CMC nanoparticles via the ratio of flow rates by central focusing. (A) Hydrodynamic diameter of nanoparticles vs R_{cf} for 5 mM (red) and 7.5 mM (blue) DTAB with various CMC concentrations: 0.04 g/L (circles), 0.1 g/L (diamonds), and 0.2 g/L (squares). Error bars are mostly hidden by the symbols. (B) Polydispersity index (PDI) of nanoparticles averaged over the three concentrations of CMC at 5 mM DTAB.

nanoparticles as a function of R_{cf}. The ratio of flow rates clearly allowed a fine control over the size of nanoparticles: as it decreased, the size smoothly increased. Besides the kinetic effect mentioned previously, another effect of R_{cf} is the change of the final concentration of both DTAB and CMC collected at the outlet. Indeed, DTAB final concentration varied as $R_{cf}/(1 + R_{cf})$, whereas CMC final concentration as $1/(1 + R_{cf})$ and was therefore more strongly affected by R_{cf}. As a rule of thumb, the nanoparticle size strongly increased with DTAB concentration but mildly decreased with an increase of CMC concentration

dx.doi.org/10.1021/ac4006155 | Anal. Chem. 2013, 85, 5850−5856

(see results below). This behavior was consistent with bulk experiments, even though the effect of CMC concentration was weaker,[27] and can explain in part the size increase of nanoparticles with R_{cf} since the final CMC concentration was accordingly diminished. Notice that an opposite variation of the nanoparticle size with R_{cf} was observed for the nanoprecipitation of polymeric particles.[19]

Figure 6B shows the PDI of nanoparticles averaged over three CMC concentrations for a DTAB concentration of 5 mM. The size distribution became narrower at increasing ratio of flow rates. The shorter mixing time τ_{mix} associated with larger R_{cf} values allowed an homogeneous binding of DTAB molecules to CMC chains yielding uniform size distributions.

Influence of Surfactant and Polyelectrolyte Concentrations. A phase diagram can be established theoretically giving the size distribution of salt-free nanoparticles as a function of the concentrations in surfactant and polyelectrolyte.[6] In practice though, the system is rarely at equilibrium especially when strong electrostatic interactions are involved, and the mixing kinetics come into play. This can be understood from Figure 7A by considering the data obtained with 5 mM

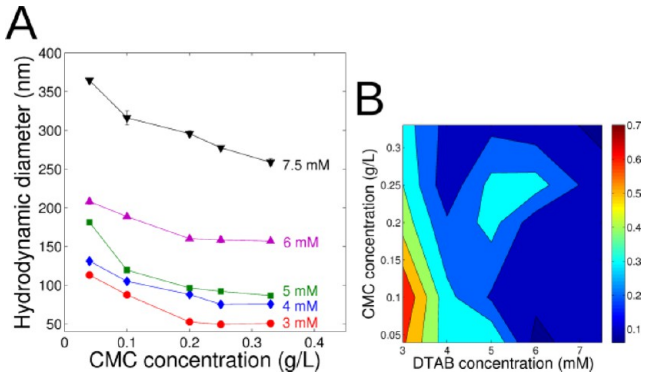

Figure 7. DTAB−CMC nanoparticles assembled at R_{cf} = 12 by central focusing. (A) Hydrodynamic diameter as a function of CMC concentration for various concentrations of DTAB: 3 mM (red discs), 4 mM (blue diamonds), 5 mM (green squares), 6 mM (magenta upper triangles), and 7.5 mM (black lower triangles). (B) Polydispersity index vs DTAB and CMC concentrations.

DTAB: the nanoparticles formed at R_{cf} = 12 and 0.2 g/L of CMC had a size identical to those formed at R_{cf} = 4 and 0.04 g/L of CMC. A simple calculation reveals similar DTAB final concentrations in both cases but CMC final concentrations had almost a 10-fold difference. This finding gives another evidence of a kinetic effect associated to R_{cf}: the hydrodynamic flow focusing not only ensured repeatable experiments through a robust mixing procedure—repeatability that is not readily achieved in bulk experiments—but it also affected the size of nanoparticles via the mixing time τ_{mix}.

As mentioned earlier, the increase of DTAB concentration led to larger nanoparticles (Figure 7A). The presence of oppositely charged polyelectrolyte promotes the accretion of surfactant[6] and acts as a nucleus on which a nanoparticle can grow by addition of free surfactant. At a given surfactant concentration, a higher number of polyelectrolyte chains gives rise to more of these nuclei, each of which has thereby fewer surfactant molecules bound to it. Consequently, the size of nanoparticle decreased with increasing CMC concentration (Figure 7A).

Figure 7B depicts the variations of polydispersity with the concentrations of polyelectrolyte and surfactant. As can be noticed, increasing the concentrations led to a smaller PDI.

Influence of Fluid Velocity. The influence of fluid velocity was studied by varying separately the flow rates of DTAB and CMC, while keeping their ratio constant at R_{cf} = 12. The results are summarized in Table 1. It can be noticed that the variations

Table 1. Size and PDI of Surfactant−Polyelectrolyte Nanoparticles Assembled at Various Flow Rates by Central Focusing while Maintaining R_{cf} = 12

		flow rates (DTAB/CMC) (μL/min)		
parameter	concentrations DTAB/CMC	24/2	36/3	48/4
size (nm)	5 mM/0.2 g/L	92.7	93.5	96.5
	5 mM/0.1 g/L	126	121	119
PDI	5 mM/0.2 g/L	0.09	0.079	0.10
	5 mM/0.1 g/L	0.17	0.15	0.19

of size and even the variations of PDI are similar, the fluid velocities having barely any influence on these quantities. The results underline that the assembly of nanoparticles is strongly influenced by the concentrations of reagents and the mixing kinetics but is marginally affected by the fluid velocity. This finding demonstrated that the assembly reaction was completed while flowing through the channel.

Morphology of the Nanoparticles. Electron microscopy images confirmed the good regularity of the nanoparticle size and were consistent with the measurements by DLS (Figure 8A). Surprisingly though, they were not spherical but rather faceted. Figure 8B depicts a large nanoparticle (~115 nm × 95 nm in size) obtained at R_{cf} = 12, which exhibits a hexagonal crystal-like shape with sharp edges. Figure 8C gives another example of an irregular but also faceted nanoparticle. Nizri et al. investigated by cryoelectron microscopy the structure of similar

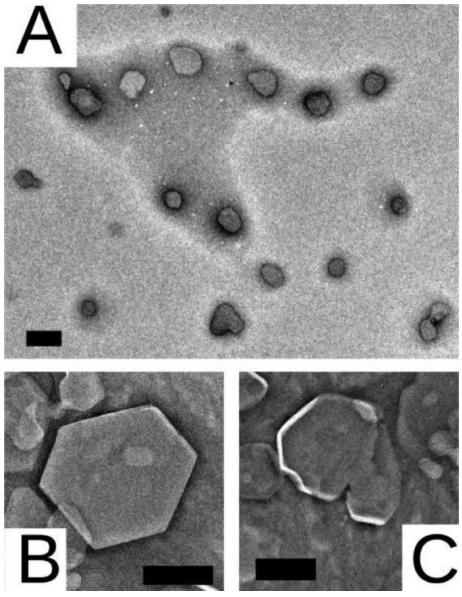

Figure 8. TEM images of DTAB−CMC nanoparticles obtained by central focusing. DTAB concentration was 5 mM. (A) CMC concentration was 0.2 g/L and R_{cf} = 8. Scale bar is 100 nm. (B and C) CMC concentration was 0.1 g/L and R_{cf} = 12. Scale bars are 50 nm.

dx.doi.org/10.1021/ac4006155 | Anal. Chem. 2013, 85, 5850−5856

systems assembled in bulk.[28] The anionic polyelectrolyte was sodium polyacrylate (NaPA), and the surfactant consisted of alkyltrimethylammonium bromide (C_nTAB) with different lengths. Interestingly, they observed aggregates of hexagonal liquid crystal with nanometric size. Their faceted shape was very similar to that of our nanoparticles except that the latter were not often perfectly hexagonal. The latter fact may be due to the nature of the polyelectrolyte as it was recently reported that CMC complexed with cationic lipids yielded shapeless nanoparticles with a disordered inner structure.[29]

CONCLUSIONS

We investigated the self-assembly of surfactant−polyelectrolyte nanoparticles assisted by hydrodynamic flow focusing in microfluidic channels. We demonstrated the importance of the kinetic effects during assembly by using two equivalent designs yielding mixing times with a 10-fold difference. It turned out that a short mixing time led to the formation of small nanoparticles. The use of microfluidics allowed the complexation of cationic surfactant and anionic polyelectrolyte with an excellent reproducibility not achievable in bulk because the charges were distributed uniformly at the mixing interface. The size of nanoparticles could be finely tuned from 50 nm to more than 300 nm by adjusting the ratio of flow rates and/or the concentrations of reagents. Images by transmission electron microscopy revealed nanoparticles with regular sizes and faceted shapes.

Assembly of nanostructures by strong interactions such as electrostatics is difficult because the process is mostly driven by kinetics at the microscale. Bulk preparations often give rise to a poor reproducibility and unpredictable size distributions. In contrast, microfluidics offers both a fine control on the mixing kinetics and a good homogeneity of charges at the interface between reagents. We therefore anticipate that microfluidics will be of great utility for assembling kinetically driven nanoparticles such as polyelectrolyte-based complexes used in colloidal industry or as vectors for gene delivery.

AUTHOR INFORMATION

Corresponding Author

*E-mail: guillaume.tresset@u-psud.fr (G.T.); ciliescu@ibn.a-star.edu.sg (C.I.). Phone: +33 1 69 15 53 60 (G.T.); +65 6824 7137 (C.I.). Fax: +33 1 69 15 60 86 (G.T.).

Notes

The authors declare no competing financial interest.

ACKNOWLEDGMENTS

The authors thank Dominique Langevin for stimulating discussions as well as Jéril Degrouard and Shrinivas Venkataraman for their assistance with transmission electron microscopy. The research was partly funded by the France−Singapore Merlion program (project reference 8.02.10), by the Agency for Science, Technology, and Research (A*STAR) in Singapore, and by CNRS through the "Interface Physique, Chimie, Biologie" program. C.M. acknowledges support from contract O.2.1.2, no.209, ID 665.

REFERENCES

(1) Goddard, E. D.; Ananthapadmanabhan, K. P. *Interaction of Surfactants with Polymers and Proteins*; CRC Press: Boca Raton, FL, 1993.
(2) Langevin, D. *Adv. Colloid Interface Sci.* **2009**, *147−148*, 170−177.
(3) Stubenrauch, C.; Albouy, P.-A.; Klitzing, R. v.; Langevin, D. *Langmuir* **2000**, *16*, 3206−3213.
(4) Huang, L.; Hung, M. C.; Wagner, E. *Non Viral Vectors for Gene Therapy*; Academic Press: New York, 1999.
(5) Chittimalla, C.; Zammut-Italiano, L.; Zuber, G.; Behr, J.-P. *J. Am. Chem. Soc.* **2005**, *127*, 11436−11441.
(6) Kuhn, P. S.; Diehl, A. *Phys. Rev. E* **2007**, *76*, 041807.
(7) Trabelsi, S.; Guillot, S.; Ritacco, H.; Boué, F.; Langevin, D. *Eur. Phys. J. E* **2007**, *23*, 305−311.
(8) Marre, S.; Jensen, K. F. *Chem. Soc. Rev.* **2010**, *39*, 1183−1202.
(9) Valencia, P. M.; Farokhzad, O. C.; Karnik, R.; Langer, R. *Nat. Nanotechnol.* **2012**, *7*, 623−629.
(10) Qi, A.; Chan, P.; Ho, J.; Rajapaksa, A.; Friend, J.; Yeo, L. *ACS Nano* **2011**, *5*, 9583−9591.
(11) Khan, S. A.; Duraiswamy, S. *Lab Chip* **2012**, *12*, 1807−1812.
(12) Belliveau, N. M.; Huft, J.; Lin, P. J.; Chen, S.; Leung, A. K.; Leaver, T. J.; Wild, A. W.; Lee, J. B.; Taylor, R. J.; Tam, Y. K.; Hansen, C. L.; Cullis, P. R. *Mol. Ther.—Nucleic Acids* **2012**, *1*, e37.
(13) Kim, Y.; Lee Chung, B.; Ma, M.; Mulder, W. J. M.; Fayad, Z. A.; Farokhzad, O. C.; Langer, R. *Nano Lett.* **2012**, *12*, 3587−3591.
(14) Knight, J. B.; Vishwanath, A.; Brody, J. P.; Austin, R. H. *Phys. Rev. Lett.* **1998**, *80*, 3863−3866.
(15) Jahn, A.; Vreeland, W. N.; Gaitan, M.; Locascio, L. E. *J. Am. Chem. Soc.* **2004**, *126*, 2674−2675.
(16) Hong, J. S.; Stavis, S. M.; DePaoli Lacerda, S. H.; Locascio, L. E.; Raghavan, S. R.; Gaitan, M. *Langmuir* **2010**, *26*, 11581−11588.
(17) Rondeau, E.; Cooper-White, J. J. *Langmuir* **2008**, *24*, 6937−6945.
(18) Majedi, F. S.; Hasani-Sadrabadi, M. M.; Emami, S. H.; Shokrgozar, M. A.; VanDersarl, J. J.; Dashtimoghadam, E.; Bertsch, A.; Renaud, P. *Lab Chip* **2013**, *13*, 204−207.
(19) Karnik, R.; Gu, F.; Basto, P.; Cannizzaro, C.; Dean, L.; Kyei-Manu, W.; Langer, R.; Farokhzad, O. C. *Nano Lett.* **2008**, *8*, 2906−2912.
(20) Tresset, G.; Takeuchi, S. *Biomed. Microdevices* **2004**, *6*, 213−218.
(21) Tresset, G.; Iliescu, C. *Appl. Phys. Lett.* **2007**, *90*, 173901.
(22) Choudhury, D.; van Noort, D.; Iliescu, C.; Zheng, B.; Poon, K.-L.; Korzh, S.; Korzh, V.; Yu, H. *Lab Chip* **2012**, *12*, 892−900.
(23) Berne, B. J.; Pecora, R. *Dynamic Light Scattering*; Dover Publications: New York, 2000.
(24) Lee, G. B.; Chang, C. C.; Huang, S. B.; Yang, R. J. *J. Micromech. Microeng.* **2006**, *16*, 1024−1032.
(25) Decher, G. *Science* **1997**, *277*, 1232−1237.
(26) Johnson, B. K.; Prud'homme, R. K. *Phys. Rev. Lett.* **2003**, *91*, 118302.
(27) Trabelsi, S.; Raspaud, E.; Langevin, D. *Langmuir* **2007**, *23*, 10053−10062.
(28) Nizri, G.; Makarsky, A.; Magdassi, S.; Talmon, Y. *Langmuir* **2009**, *25*, 1980−1985.
(29) Tresset, G.; Lansac, Y.; Romet-Lemonne, G. *Langmuir* **2012**, *28*, 5743−5752.